

Computational Analysis of Electrical Impedance Spectroscopy for Margin Tissue Detection in Laparoscopic Liver Resection

Sulistia Sulistia^a, Riyanto Riyanto^b, Pratondo Busono^c, Affandi Faisal Kurniawan^a,
Joko Saefan^a, Wawan Kurniawan^a, Marlin Ramadhan Baidillah^{b,*}

^aPhysics Education

Universitas PGRI Semarang

Jl. Sidodadi Timur Jalan Dokter Cipto No. 24
Semarang, Indonesia

^bResearch Center for Electronics

National Research and Innovation Agency (BRIN)
KST Samaun Samadikun

Bandung, Indonesia

^cResearch Center for Smart Mechatronics

National Research and Innovation Agency (BRIN)
KST Samaun Samadikun
Bandung, Indonesia

Abstract

Margin tissue detection during intraoperative laparoscopic liver resection (LLR) is required to prevent tumor recurrence and reduce the likelihood of further surgery. This study proposes an electrical impedance spectroscopy (EIS) method for margin tissue detection in LLR to determine the boundary interface of normal and cancerous tissue. This study has three objectives: (1) designs the electrode array configuration to collect multiple EIS impedance measurements, (2) implements the Feedforward Neural Network (FNN) to classify the orientation of margin tissue relative to the electrode array by using time-difference impedance indexes, and (3) governs the inflection point method based on impedance indexes to detect the margin tissue location. The proposed method was evaluated by a 3D numerical simulation of liver tissue composed of cancerous lumps with $I_{ac} = 1$ mA alternating injection current at frequencies $lf = 1$ kHz and $hf = 100$ kHz. The electrode array consists of 16 electrode pairs each for injection current and voltage measurements. The variation of margin tissue orientation relative to the electrode array direction was considered to occur in unidirectional, perpendicular, and diagonal direction with noise variations (Signal-to-Noise-Ratio: 50 to 90 dB). The FNN trained on 2,400 data points achieves True Positive Rate (TPR) value of 90.2%, 99.4%, and 96.6% for diagonal, perpendicular, and unidirectional respectively in margin tissue orientation classification, while the inflection point method detects margin tissue location with 75% location at the unidirectional orientation (y -axis).

Keywords: Laparoscopy liver resection, Electrical impedance spectroscopy, Machine learning algorithm, Time-difference Impedance indexes, Margin tissue detection.

I. INTRODUCTION

The global prevalence of liver cancer has been steadily rising, resulting in it being ranked as the fourth leading cause of death worldwide and accounting for more than 800,000 deaths each year [1], [2]. Liver cancer is a prominent contributor to global cancer mortality, resulting in over 700,000 fatalities annually. The high prevalence of liver cancer requires an urgent focus on the development of innovative therapy and monitoring techniques. The intricate hepatic vascular structure and the variability of lesion locations make

liver cancer surgery a high-risk treatment. The utilization of laparoscopic liver resection (LLR) has demonstrated encouraging outcomes in terms of decreased need for blood transfusions during surgery and a shorter duration of hospitalization. LLR is a minimally invasive surgical procedure used to remove benign or cancerous liver lesions. It involves making small incisions through which specialized instruments and a camera are inserted to perform the resection. LLR offers several advantages over traditional open liver resection, including faster postoperative recovery, reduced blood loss, shorter hospital stays, and better cosmetic results [3]. The importance of laparoscopic liver resection lies in its ability to provide patients with a less invasive treatment option for liver lesions, leading to faster recovery, reduced pain, and improved cosmetic outcomes. Additionally, LLR has been shown to have

* Corresponding Author.

Email: marlin.ramadhan.baidillah@brin.go.id

Received: February 15, 2024 ; Revised: April 19, 2024

Accepted: April 23, 2024 ; Published: August 31, 2024

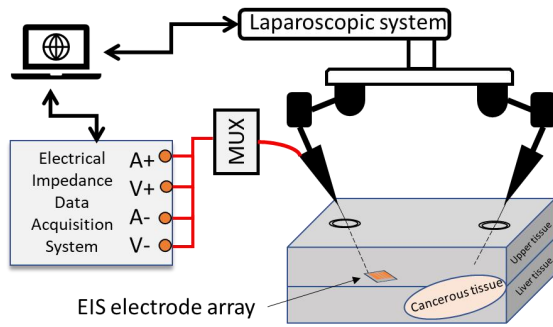


Figure 1. The conceptual procedure of margin tissue detection based on electrical impedance spectroscopy.

lower postoperative mortality and morbidity rates compared to open liver resection, making it a favorable option for many patients [3], [4].

The implementation of a novel monitoring method in LLR for intraoperative liver cancer to determine the margin tissue location is crucial for enhancing surgical results, minimizing complications, and yielding substantial economic ramifications [5], [6]. Margin tissue assessment is the process of assessing the boundary between healthy and unhealthy tissue selected for surgery. It refers to the shortest distance between the edges of the tumor and the surrounding non-cancerous tissue in the liver section. This assessment is critical to ensure that unhealthy tissue is removed in its entirety. The adequacy of this margin is crucial in determining the completeness of the resection and has implications for patient outcomes, including the risk of recurrence and survival rates. This assessment may involve various methods, including assessment of resection margin width and anatomical quality [7]. Some studies suggest that a more complete assessment of the margins may assist the veterinarian or human doctor in determining whether the neoplasm has been completely removed. The margin valuation method used can affect the level of positive margin and the total volume of tissue lifted [8]. The challenge of margin tissue determination is that both normal and cancerous tissues have similar colors. Thus, determination by using only a camera may show an inaccurate result, lack of depth detection, and need a contrast agent [9], [10].

Several studies have proposed the use of Electrical Impedance Spectroscopy (EIS) for tissue identification, which has a potential application for margin tissue assessment. Halter et al. [11], Mahara et al. [12], and Murphy et al. [13] examined the use of imaging of conductivity distribution with radially configured microendoscopic electrical impedance probes with 17 electrodes with a frequency range from 10 kHz to 1 MHz and tetrapolar electrical impedance measurement. Even though it was not clear to determine the clear boundary of the margin tissue by using the reconstructed conductivity distribution, it showed the capability to determine the inclusion of a 1 mm diameter with a conductivity contrast ratio of 10:1 as compared to the background's conductivity. The study of Cheng et al. [14] used tripolar electrical impedance measurement to calculate the conductivity and

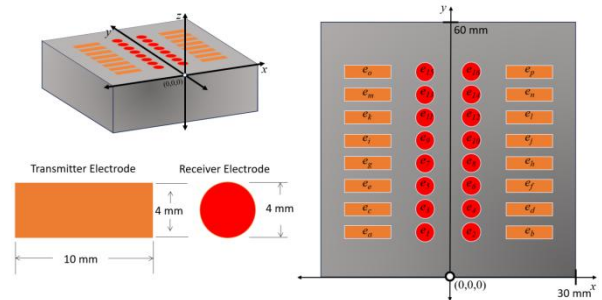


Figure 2. The proposed design of the electrode array configuration for electrical impedance spectroscopy.

permittivity values of the assessed tissue with a frequency range from 1 kHz to 349 kHz by moving the voltage measurement electrode using a robotic arm at a specific distance. The results showed that different tissues can be identified consistently with variation distance, but it was not shown how this method can be used to identify the margin tissue. Doussan et al. [15] reported the development of an electrical impedance-based probe with 32 electrodes, a 12 mm diameter, and a frequency range from 100 Hz to 1 MHz to generate 3D images of the tissue and classify between muscle and adipose tissue. The study identified the positive surgical margins (PSMs) in real-time during radical prostatectomy (RP) surgery until 1.19 mm depth. Since the middle area of the electrical impedance-based probe is the most accurate for reconstructing the image, the study did not show the margin tissue image's accuracy for the other areas.

In this study, we propose using electrical impedance spectroscopy (EIS) for margin assessment during laparoscopic surgery. To obtain the margin tissue location, we conduct three objective studies by first implementing ratio metric profiles in the proposed electrode array configuration design. The ratio metric profile is the ratio of impedance MIX, phase PIX, real part impedance RIX, and imaginary part impedance IMIX at two different frequencies that are chosen solely based on the characteristic relaxation of biological tissues at the lower frequency lf and higher frequency hf . The aim of using the ratio metric is to reduce the unnecessary data training required for machine learning. Secondly, the margin tissue orientation can be classified by implementing the Feedforward Neural Network (FNN) model and impedance indexes (MIX, RIX, and IMIX). Lastly, the margin tissue location at the impedance index curve is detected by proposing the inflection point method.

II. EIS ASSISTED IMPEDANCE INDEXES AND MACHINE LEARNING FOR MARGIN TISSUE DETECTION

Figure 1 shows the conceptual procedure for margin tissue detection in LLR based on EIS and the position of the EIS electrode array in the laparoscopic probe. The electrode array is attached to one of the laparoscopic probes and the electrical impedance data acquisition system. The impedance data from EIS is

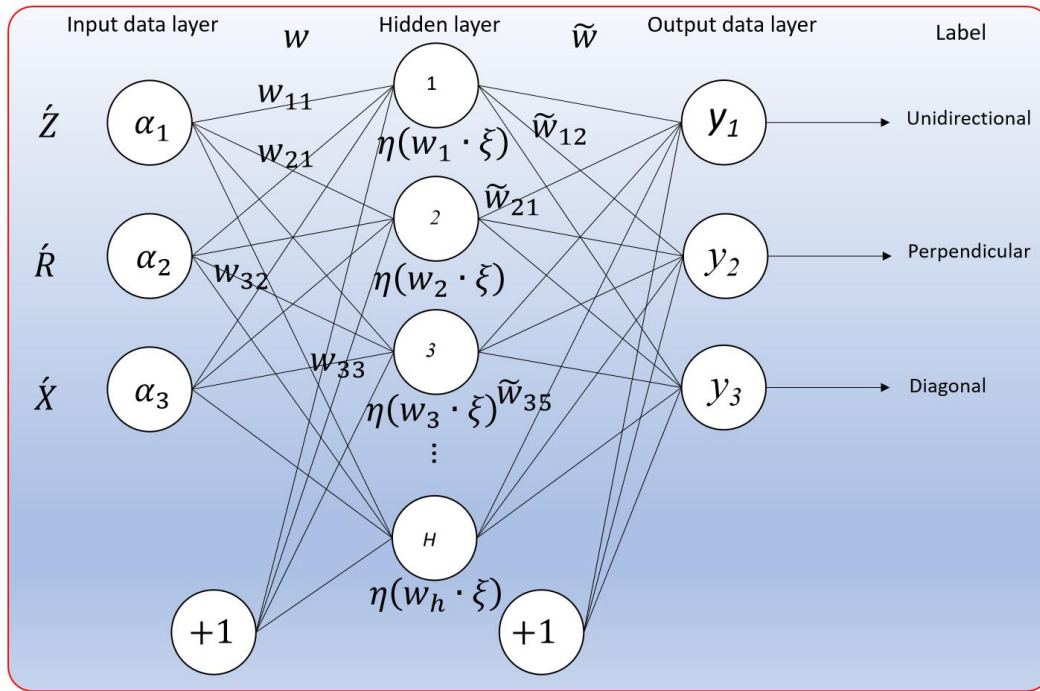


Figure 3. The schematic flow of margin tissue orientation classification by FNN.

collected at two different frequencies (low frequency lf and high frequency hf), which are selected according to their relaxation behavior between normal and cancerous tissue. The impedance indexes of these impedance data are then used in the FNN to determine the orientation of margin tissue relative to the electrode array direction. The orientation of margin tissue can be perpendicular, unidirectional, or diagonal relative to the electrode array direction. If the margin tissue orientation is ‘unidirectional’, then the margin tissue location is detected by using the inflection point method. Otherwise, the electrode array should be rotated until the results of FNN are ‘unidirectional.’

A. Electrode Array Configuration

The EIS electrode array configuration proposed in this study is depicted in Figure 2, also included in Figure 1. The dimension of the electrode array is limited by the size allowed for the laparoscopy probe during the intraoperative surgery. The space among the electrodes is also designed to be equal to the dimension of each electrode in order to avoid surface current due to the narrow space between the adjacent electrodes. The electrode array is designed in a vertical array in order to specify the margin tissue location that is unidirectional to the electrode array.

The electrode array is composed of four columns and eight rows, with 16 electrode pairs for each current injection and voltage measurement. The electrode shape of the current injection is relatively larger in size than that of the voltage measurement to increase the current density between the current injection electrode pair, thus increasing the sensitivity of the voltage measurement. The scanning measurement protocol can be seen in Table I. The first scanning measurement is the electrode pair $e_a - e_b$ as the current injection and $e_1 - e_2$ until $e_{15} -$

e_{16} as the voltage measurement. There are 64 impedance measurement numbers in total.

B. Feature extraction by impedance indexes

In order to minimize the unnecessary data training of FNN, this study implements two impedance indexes as a data feature extraction, which are magnitude index MIX, real-part index RIX, and imaginary part index IMIX, as suggested by Ibrahim et al. [16]. Considering that the conductivity change source classification is a time-domain analysis, thus, the two impedance indexes in the time-domain analysis are formulized in (1) to (6).

$$MIX = \frac{\dot{Z}_t - \dot{Z}_{t_0}}{\dot{Z}_{t_0}} \quad (1)$$

$$RIX = \frac{\dot{R}_t - \dot{R}_{t_0}}{\dot{R}_{t_0}} \quad (2)$$

$$IMIX = \frac{\dot{X}_t - \dot{X}_{t_0}}{\dot{X}_{t_0}} \quad (3)$$

where,

$$\dot{Z} = \frac{\text{abs}(Z_{lf})}{\text{abs}(Z_{hf})} \quad (4)$$

$$\dot{R} = \frac{\text{re}(Z_{lf})}{\text{abs}(Z_{hf})} \quad (5)$$

$$\dot{X} = \frac{\text{im}(Z_{lf})}{\text{abs}(Z_{hf})} \quad (6)$$

t is an arbitrary unit of time after a reference time t_0 , $\text{abs}(Z)$ is the magnitude (modulus) of the complex electrical impedance, $\text{re}(Z)$ is the real part of the complex electrical impedance ($\text{re}(Z) = \text{abs}(Z) \cdot \cos[\arg(Z)]$), and $\text{im}(Z)$ is the imaginary part of the complex electrical impedance ($\text{im}(Z) = \text{abs}(Z) \cdot \sin[\arg(Z)]$). While, \dot{Z} , \dot{R} , and \dot{X} are the ratio between $\text{abs}(Z)$, $\text{re}(Z)$, and $\text{im}(Z)$ as compared with the magnitude (modulus) of the complex electrical impedance at the hf .

TABLE I. ELECTRICAL IMPEDANCE MEASUREMENT PROTOCOL.

Measurement Number	Current Injection Pair		Voltage Measurement Pair	
1	e _a	e _b	e ₁	e ₂
2			e ₃	e ₄
3			e ₅	e ₆
4			e ₇	e ₈
5			e ₉	e ₁₀
6			e ₁₁	e ₁₂
7			e ₁₃	e ₁₄
8			e ₁₅	e ₁₆
9	e _c	e _d	e ₁	e ₂
10			e ₃	e ₄
11			e ₅	e ₆
12			e ₇	e ₈
13			e ₉	e ₁₀
14			e ₁₁	e ₁₂
15			e ₁₃	e ₁₄
16			e ₁₅	e ₁₆
17	e _e	e _f	e ₁	e ₂
18			e ₃	e ₄
19			e ₅	e ₆
20			e ₇	e ₈
21			e ₉	e ₁₀
22			e ₁₁	e ₁₂
23			e ₁₃	e ₁₄
24			e ₁₅	e ₁₆
25	e _g	e _h	e ₁	e ₂
26			e ₃	e ₄
27			e ₅	e ₆
28			e ₇	e ₈
29			e ₉	e ₁₀
30			e ₁₁	e ₁₂
31			e ₁₃	e ₁₄
32			e ₁₅	e ₁₆
33	e _i	e _j	e ₁	e ₂
34			e ₃	e ₄
35			e ₅	e ₆
36			e ₇	e ₈
37			e ₉	e ₁₀
38			e ₁₁	e ₁₂
39			e ₁₃	e ₁₄
40			e ₁₅	e ₁₆
41	e _k	e _l	e ₁	e ₂
42			e ₃	e ₄
43			e ₅	e ₆
44			e ₇	e ₈
45			e ₉	e ₁₀
46			e ₁₁	e ₁₂
47			e ₁₃	e ₁₄
48			e ₁₅	e ₁₆
49	e _m	e _n	e ₁	e ₂
50			e ₃	e ₄
51			e ₅	e ₆
52			e ₇	e ₈
53			e ₉	e ₁₀
54			e ₁₁	e ₁₂
55			e ₁₃	e ₁₄
56			e ₁₅	e ₁₆
57	e _o	e _p	e ₁	e ₂
58			e ₃	e ₄
59			e ₅	e ₆
60			e ₇	e ₈
61			e ₉	e ₁₀
62			e ₁₁	e ₁₂
63			e ₁₃	e ₁₄
64			e ₁₅	e ₁₆

These matrix profiles do not assume any tissue model and solely consider fundamental physical aspects of the behavior of electrical impedance in the selected frequency range [17], [18]. Thus, the accuracy of (1) to

(3) depends on the lower frequency lf and higher frequency hf selections.

C. Classifier by Feedforward Neural Network (FNN)

The impedance data is nonlinearly affected by the location and orientation of the margin tissue relative to the electrode array. Both orientation and location of the margin tissue are the sources of impedance change in EIS measurement. To accurately determine the location of the margin tissue, the orientation of the margin tissue must be determined first. In order to determine the location and orientation of margin tissue, imaging of conductivity distribution can be used, as shown by the Electrical Impedance Tomography (EIT) method [19]. However, the measurement protocol should be increased in order to obtain an accurate image, thus leading to a more complicated electrical impedance circuit that is not suitable for a laparoscopic system.

In this study, margin tissue orientation is classified using the feedforward neural network (FNN), as shown in Figure 3. The trained classifier of FNN is a fully connected layer of the neural network and connections from the network inputs to each subsequent layer from the previous layer, also called multi-layer perceptron (MLP). The structure of FNN has one hidden layer with 100 neurons, the two impedance indexes as data input in the input layer, and the three-label data as data output in the output layer. This fully connected FNN structure has $(\xi \times h) + (h \times o)$ total number of weight connections, where $\xi = \{1, \dots, \mathcal{E}\}$ is data input in the input layer, $h = \{1, \dots, H\}$ is a neuron in the hidden layer, and $o = \{1, \dots, O\}$ is the number of data output in the output layer. The weight connections are used to perform the computation. The computation steps of the network of one hidden layer FNN for the n th sample of the trained dataset are as follows:

- the first step (7) is summing the weights in the hidden layer:

$$S_h^n = \sum_1^H w_{h\xi} \alpha_\xi + \beta_\xi \quad (7)$$

where α_ξ is the input data (which are impedance indexes), $w_{h\xi}$ is the weight vector connecting the input neurons ξ th and the hidden layer neuron h th, and β_ξ is the input variable's bias term,

- the second step (8) is feeding the summations of the first step NN computation to the neurons' output by using the rectified linear unit (ReLU) activation function f_h :

$$f_h(S_h^n) = \begin{cases} S_h^n, & S_h^n > 0 \\ 0, & S_h^n \leq 0 \end{cases} \quad (8)$$

where S_h^n is the sum of weights,

- the last step (9) is calculating the output neurons:

$$y_o^n = \sum_1^H \tilde{w}_{ho} f_h + \beta_h \quad (9)$$

where y_h^n is the output of hidden layer neuron h th, \tilde{w}_{ho} is the weight between the output variable y_o^n and hidden layer neuron h th, β_h is the output variable's bias term, n is the number of samples which is F (number of frequency pair of lower frequency lf and higher frequency hf) times t (number of impedance measurements in a time domain), $F = \{1, \dots, F\}$, and $t = \{1, \dots, T\}$.

In order to obtain the classifier, the training process based on supervised learning employs a tuning process to control the weight ($w_{h\xi}$ and \tilde{w}_{ho}) and bias (β_ξ and β_h) parameters based on the minimizing error rate, including both classification and approximation errors.

III. NUMERICAL SIMULATION STUDIES

A. Forward problem

Figure 4 shows the geometry of the liver model with EIS electrodes, which liver cancerous tissue presents. The contact impedance on each electrode is $Z_c = 50 \Omega$. Meanwhile, the electrical properties of liver normal and cancerous tissues are referred to in the literature [20], [21]. The selection of two frequencies of lf and hf is decided where the spectrum of the cancerous tissue has a distinct value from the normal one; see Table II [22], [23].

To generate a dataset for training, we have solved the forward problem by employing a finite element method (FEM) simulation of electrical potential $\phi(\mathbf{r})$ inside a subdomain Ω when a current across the surface of the liver in boundary $\partial\Omega$ is applied on each electrode of current injection I [24] using (10) to (13).

$$\nabla \cdot (\gamma(\mathbf{r})) \nabla \phi(\mathbf{r}) = 0, \quad \mathbf{r} \in \Omega \quad (10)$$

$$\phi(\mathbf{r}) + Z_c \gamma(\mathbf{r}) \frac{\partial \phi(\mathbf{r})}{\partial \mathbf{n}} = U_l, \quad \mathbf{r} \in e_l, \quad l = \{1, \dots, L\} \quad (11)$$

TABLE II. ELECTRICAL PROPERTIES COMPARISON BETWEEN NORMAL AND CANCEROUS LIVER TISSUE [22], [23].

Frequency y_f [kHz]	Conductivity σ [S/m]		Relative permittivity ϵ_r [-]	
	Normal tissue	Cancerous Tissue	Normal tissue	Cancerous Tissue
1	0.1	0.28	127581	127581
10	0.11	0.30	49957	49957
100	0.17	0.35	11064	11064
1000	0.3	0.44	1859	1859

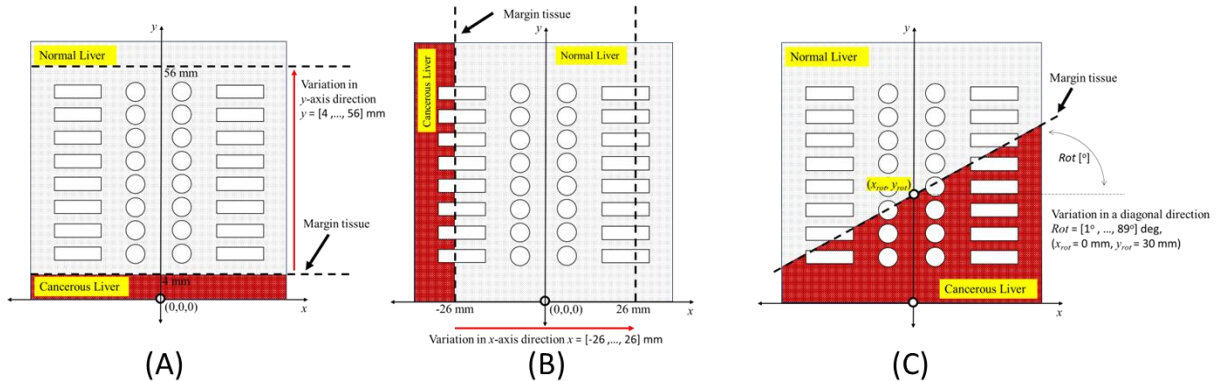


Figure 4. The electrode array configuration of forward model for three different geometries of liver model with cancerous tissue from the xy -axis point of view.

$$\int_{e_l} \gamma(\mathbf{r}) \frac{\partial \phi(\mathbf{r})}{\partial \mathbf{n}} dS = I, \quad \mathbf{r} \in \partial\Omega \quad (12)$$

$$\gamma(\mathbf{r}) \frac{\partial \phi(\mathbf{r})}{\partial \mathbf{n}} = 0, \quad \mathbf{r} \in \partial\Omega \setminus \cup_{l=1}^L e_l \quad (13)$$

where, $\gamma := \sigma + 2\pi f \epsilon \in \mathbb{C} [\text{S m}^{-1}]$ is the non-homogeneous admittivity property of liver tissues, σ and ϵ are the conductivity [S/m] and absolute permittivity [F/m], respectively in Ω at the frequency f , $\phi(\mathbf{r}) \in \mathbb{C} [\text{V}]$ is the electrical potential distribution, $\mathbf{r} := (x, y, z)$ is the coordinate system in subdomain Ω , the electrode number, length, voltage, current, and contact impedance of the l th electrode are represented by L , dS , U_l , I and Z_c , respectively. The comparison of conductivity $\sigma(\mathbf{r})$ and relative permittivity $\epsilon_r(\mathbf{r})$ of each layer are shown in Table II.

A 3D tetrahedral mesh is used to discretize the forward problem and solve it using a FEM with electrodes defined by faces in the 3D mesh [25]. The procedure is repeated for each current injection and voltage measurement electrode pair at different frequencies. The meshing process is conducted via an open-source software suite for image reconstruction in electrical impedance tomography and diffuse optical tomography (EIDORS) in Matlab [26].

B. Dataset Training

1) Variation of conductivity value

The variation of the conductivity value of liver normal tissue is selected at frequencies $lf = 1$ kHz and $hf = 100$ kHz according to the literature, which is $s_{lf} = 0.1$ S/m and $s_{hf} = 0.2$ S/m [22], [23]. In contrast, the conductivity value of liver cancerous tissue is defined as about four times higher than the normal one [22], [23]. At these frequencies, the gradient conductivity of liver normal tissue and cancerous tissue is quite distinct, which leads to a high possibility of determination using impedance measurement. However, no known works of literature suggest the selection of specific lf and hf values due to variations of signal-to-noise ratio (SNR) for different EIS systems and unknown parasitic noises. Thus, lf and hf can vary and shall be traced along with the frequency range. This assumption is also supported by [27]–[29], which indicates that gradient conductivity may vary over time. In this regard, a multi-frequency EIS measurement shall be conducted during the experiment to catch the difference between normal tissue and cancerous tissue. Multi-frequency EIS

TABLE III. NUMERICAL SIMULATION CONDITIONS.

Case Number	Variation margin tissue position/orientation		Frequency	SNR	Label
1 - 800	Unidirectional	$y = [4, \dots, 56]$ mm	$f_f = 1$ kHz & $h_f = 100$ kHz	[50, 60, 70, 80, 90] db	Unidirectional
801 - 1600	Perpendicular	$x = [-26, \dots, 26]$ mm			Perpendicular
1601 - 2400	Diagonal	$Rot = [2^\circ, \dots, 88^\circ]$, $x_{rot} = 0, y_{rot} = [15, \dots, 45]$ mm			Diagonal

measurement is also suggested by [30] to obtain the best frequency for the best conductivity visualization.

2) Variation of margin tissue orientation

Figure 4 shows the variation of margin tissue orientation relative to the electrode array configuration direction. There are three different orientations: unidirectional, perpendicular, and diagonal. Each variation is divided into two regions of tissues, which are liver normal and cancerous tissue. On each unidirectional variation, the margin tissue has variation in the y -axis direction with 400 different locations from $y = 4$ mm to 56 mm. The adjacent position of liver normal and cancerous tissue is also varied and is located either upper-bottom or bottom-upper (see Figure 4.a). Additionally, to consider the noise condition in the real practice for each measurement, each measurement was modified by adding different SNR = [50, 60, 70, 80, 90] dB. Consequently, the unidirectional orientation has 800 variation data points. The case of perpendicular orientation (see Figure 4.b) is also similar to unidirectional variation, which has 800 variation data points and has variation in the x -axis direction with 400 difference locations from $x = -26$ mm to 26 mm.

Meanwhile, in the case of diagonal orientation (see Figure 4.c), it has variation in terms of y -axis variation and rotational variation. In terms of y -axis variation, the center point of margin tissue (x_{rot}, y_{rot}) is varied with 20 different locations from $y = 15$ mm to 45 mm. In terms of rotational variation, the margin tissue is rotated from

$Rot = [2^\circ, \dots, 88^\circ]$ with 20 different rotation angles. The adjacent position of liver normal and cancerous tissue in diagonal variation is also varied, which is located either upper-bottom or bottom-upper. Thus, diagonal variation has 800 variation data points.

3) Labeling

Labeling is required in the FNN dataset training, as shown in Table III. Any impedance measurement results from the data variation of unidirectional, perpendicular, and diagonal variation is labeled as “*unidirectional*”, “*perpendicular*”, and “*diagonal*” respectively.

C. Feedforward Neural Network framework

The FNN in this paper was used as a supervised classification learner in order to classify the margin tissue orientation prior to the margin tissue location determination. The FNN was implemented by using a Matlab Machine Learning and Deep Learning Toolbox (Mathworks, Natick, MA, United States) on a laptop with CPU AMD Ryzen 7 PRO 4750U @1.7 GHz. The validation accuracy Acc [%] with k -fold = 5 is expressed in (14).

$$Acc = \frac{T_{\text{predict}}}{T_{\text{samples}}} \times 100 \quad (14)$$

where, T_{predict} is the number of true predictions, and T_{samples} is the number of total samples used in the data training.

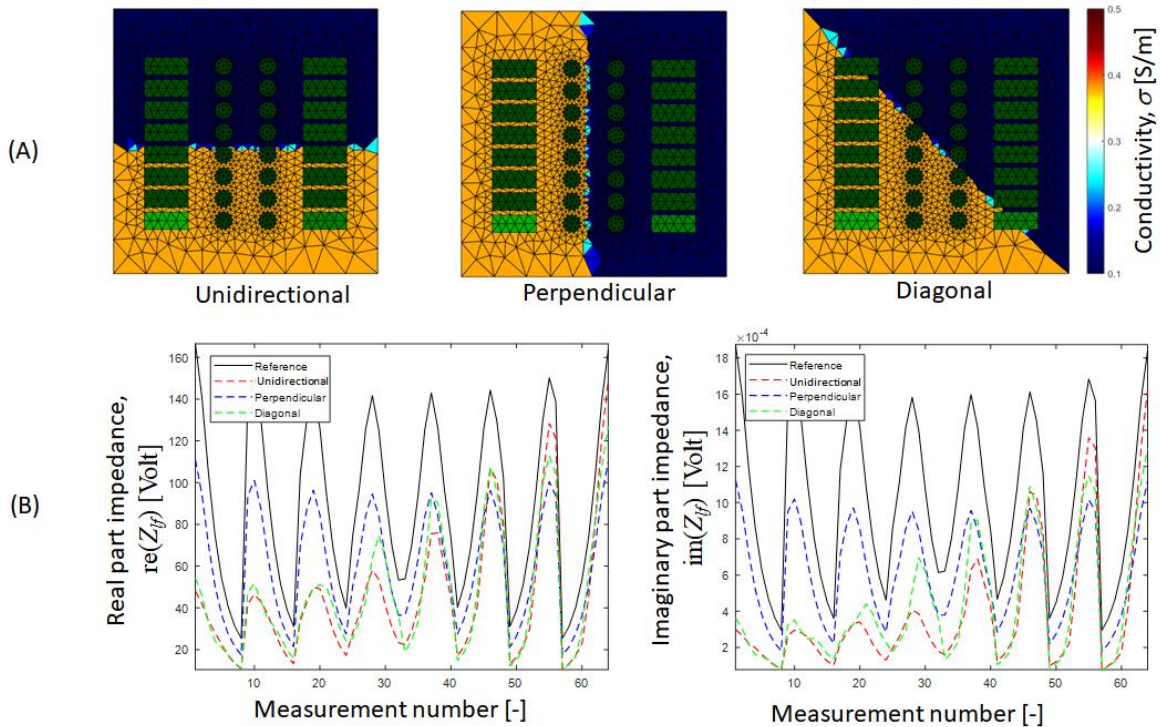


Figure 5. The comparison of real part and imaginary part of impedance under reference, unidirectional, perpendicular, and diagonal variation of margin tissue in the case of frequency $f_f = 1$ kHz and SNR = 90 db.

IV. RESULTS

A. Margin tissue orientation variation

Figure 5 shows the real part and imaginary part of impedance under unidirectional, perpendicular, and diagonal variation of margin tissue in the case of frequency $f=1$ kHz and SNR=90 db. The EIS measurement can detect the liver cancerous and normal tissue by referring to the reference measured voltage. The difference in margin tissue orientation affects the amplitude at different measurement number pairs. However, it is not trivial to decide the margin tissue location based on the comparison of measured impedance, either in terms of real or imaginary part impedance.

B. Margin tissue orientation variation classification

Figure 6 shows the performance of FNN to classify the margin tissue orientation. The true positive rate (TPR) value represents the ratio of the true prediction number as compared to the desired true prediction number. Meanwhile, the false negative rate (FNR) represents the ratio of false negatives to the total number of actual positives. The best FNN model should provide as high a TPR as possible and as low a FNR as possible. In our studies, the FNN model provides the TPR values of 90.2%, 99.4%, and 96.6% for diagonal, perpendicular, and unidirectional, respectively. Meanwhile, the FNR values are 9.8%, 0.6%, and 3.4% for diagonal, perpendicular, and unidirectional, respectively.

C. Margin tissue location determination

Figure 7 shows the comparison of impedance indexes based on MIX, RIX, and IMIX at different margin tissue locations of unidirectional orientation. The variation of each impedance index is shown to predict the margin tissue location (see the red square mark at the dashed black line). The y -axis of the MIX, RIX, and IMIX graphs indicates the number of current injection pairs. The first current injection pair is $e_a - e_b$, and the last one is $e_o - e_p$. The margin tissue location of unidirectional variation varied from $y = 11.7$ mm (at the intersection of the 1st current injection pair, i.e., $e_a - e_b$) to the $y = 48.2$ mm (at the intersection of the 8th current injection pair, i.e., $e_o - e_p$).

True Class	Diagonal	90.2%	0.9%	8.8%	Predicted Class	TPR	FNR		
	Perpendicular	0.6%	99.4%	0.0%				99.4%	0.6%
	Unidirectional	3.4%		96.6%				96.6%	3.4%
		Diagonal	Perpendicular	Unilateral					

Figure 6. The accuracy of FNN model for margin tissue orientation classification.

Considering the accuracy of margin tissue location prediction based on the inflection of the variance of impedance indexes in Figure 6, the most accurate locations are from $y = 16.5$ mm to $y = 43$ mm, which are the intersections between the 2nd and 7th current injection pairs. Thus, the proposed electrode array configuration, with the composition of eight different current injection layer, has an accuracy prediction of almost 75% location at the unidirectional orientation (y -axis).

V. DISCUSSION AND FUTURE WORKS

A. Reliability of electrode array configuration

The proposed design of electrode array configuration is reliable in detecting the variation of margin tissue location in a unidirectional direction, as shown in the results of Figure 7. The margin tissue location prediction was shown by a discrete value that represents the position of the current injection pair electrodes, because any unidirectional variation between the adjacent current injection pair will be measured at the same voltage. The most accurate current injection pairs to detect the variation of margin tissue are the 2nd to 7th pairs. The 1st and 8th current injection pairs are not accurately detecting their margin tissue locations. This is due to the fringing effect of the electric field at the edge current injection pairs. The fringing effect of an electric field is a phenomenon that occurs for electrodes with a finite length. A uniform electric field usually exists in the middle of an electrode pair; however, at the edges of the electrode pairs, the electric field becomes more non-uniform and tends to extend out into the surrounding space [31], [32].

B. Reliability of FNN

The impedance results based on margin tissue at unidirectional, perpendicular, and diagonal orientations have different features, but they are difficult to distinguish based on the qualitative analysis. The developed FNN model also already considers the variation noise condition to mimic the real-world practice conditions. The results of the developed FNN model successfully classify the margin tissue orientation with reliable accuracy.

C. Reliability of inflection point method

The location prediction of the margin tissue interface based on the proposed inflection point method showed prominent results. The inflection point method calculates the inflection point as a local minimum at the second derivative of the variance data of impedance indexes. The idea of the inflection point method is that the current penetration and electric field distribution at the interface of two dielectric mediums always propagate with the smoothing effect, and the gradient value depends strongly on the ratio of electrical properties between the adjacent mediums. Thus, any voltage measurement that is scanned from the two dielectric mediums tends to deflect.

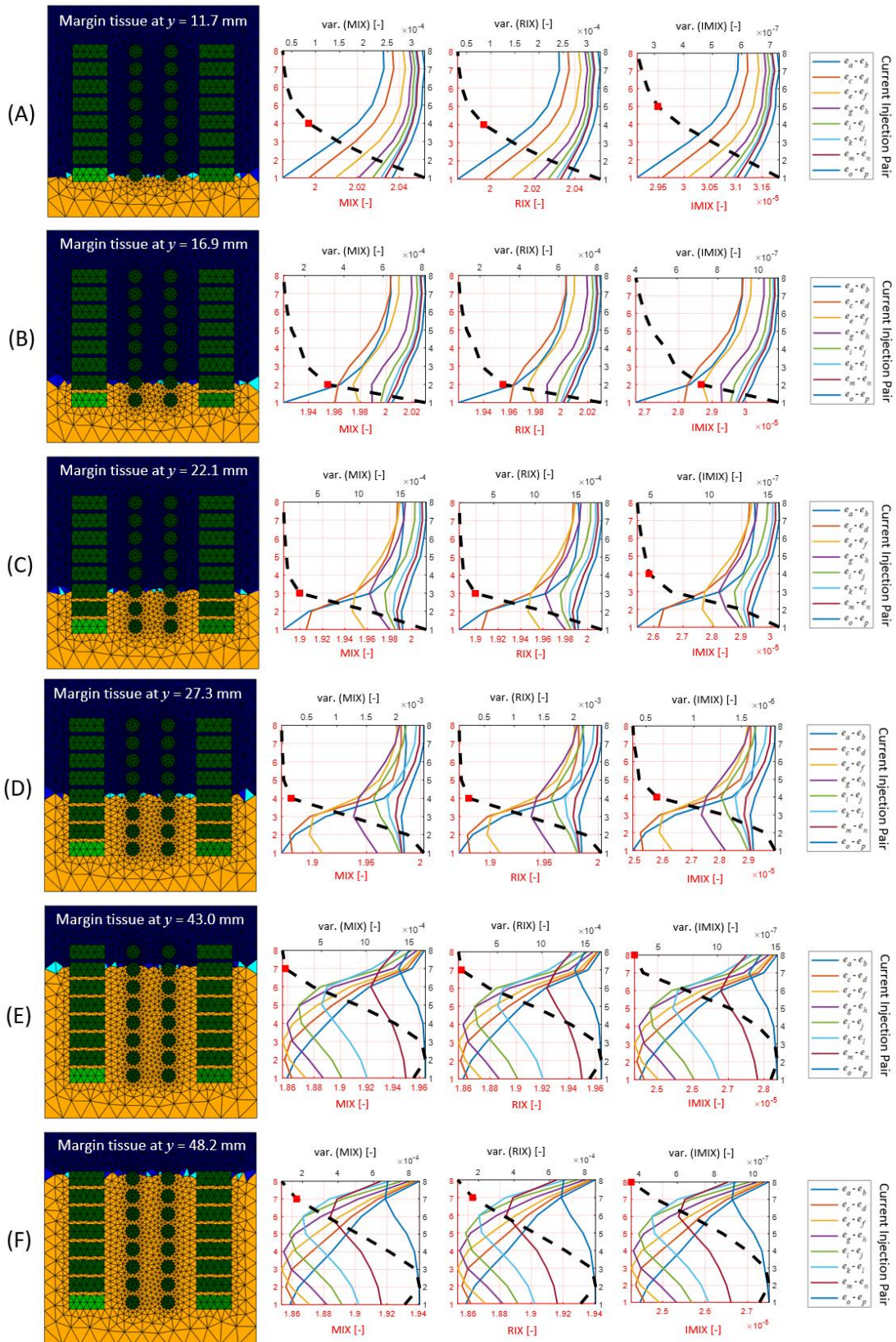


Figure 7. the comparison of impedance indexes based on MIX, RIX, and IMIX at different margin tissue location of unidirectional orientation. The margin tissue location is shown as the red square mark at the dash black line.

D. Future Works

In this study, we have shown a promising method for margin tissue detection in intraoperative laparoscopic liver resection. The study was conducted by using numerical simulation with noise condition

consideration to mimic a real practice. Further studies will be conducted by manufacturing the electrode array configuration as we designed and implementing the proposed method in the laparoscopy system.

VI. CONCLUSION

In this study, from the numerical simulation, some concluding remarks are as follows: the designed electrode array configuration detects cancerous tissue by showing the different values of real and imaginary impedance as compared with normal tissue. The margin tissue orientation significantly affects the trend line of the real part and the imaginary impedance curve. The FNN model to classify the margin tissue orientation and the impedance indexes as feature extraction successfully classifies the margin tissue orientation with a true positive rate (TPR) of 90.2%, 99.4%, and 96.6% for diagonal, perpendicular, and unidirectional, respectively. The inflection point method detects the margin tissue location with an accuracy prediction of almost 75% at the unidirectional orientation (y -axis).

DECLARATIONS

Conflict of Interest

The authors have declared that no competing interests exist.

CRediT Authorship Contribution

Sulistia Sulistia: Writing-Reviewing, Editing, Investigation, Software; Riyanto Riyanto: Funding Acquisition; Pratondo Busono: Funding Acquisition; Affandi Faisal Kurniawana: Supervision; Joko Saefana: Supervision; Wawan Kurniawan: Supervision; Marlin Ramadhan Baidillah: Conceptualization, Writing-Original draft preparation, Writing-Reviewing, Editing, Visualization, Investigation, Software.

Funding

This paper was funded by the National Agency for Research and Innovation (BRIN), Republic of Indonesia, for fiscal year 2023 (NO: 82/IL.7/HK/2022, Title: Telesurgical Robotic System).

REFERENCES

- [1] H. Rumgay *et al.*, "Global burden of primary liver cancer in 2020 and predictions to 2040," *J. Hepatol.*, vol. 77, no. 6, pp. 1598–1606, Dec. 2022, doi: 10.1016/J.JHEP.2022.08.021.
- [2] J. H. Oh and D. W. Jun, "The latest global burden of liver cancer: A past and present threat," *Clin. Mol. Hepatol.*, vol. 29, no. 2, pp. 355–357, Apr. 2023, doi: 10.3350/CMH.2023.0070.
- [3] Y. Le Linn *et al.*, "Systematic review and meta-analysis of difficulty scoring systems for laparoscopic and robotic liver resections," *J. Hepatobiliary. Pancreat. Sci.*, vol. 30, no. 1, pp. 36–59, Jan. 2023, doi: 10.1002/JHBP.1211.
- [4] C. Jia, H. Li, N. Wen, J. Chen, Y. Wei, and B. Li, "Laparoscopic liver resection: a review of current indications and surgical techniques," *Hepatobiliary Surg. Nutr.*, vol. 7, no. 4, pp. 277–288, Aug. 2018, doi: 10.21037/HBSN.2018.03.01.
- [5] H. Tugal, B. Gautier, B. Tang, G. Nabi, and M. S. Erden, "Hand-impedance measurements with robots during laparoscopy training," *Rob. Auton. Syst.*, vol. 154, Aug. 2022, Art. no. 104130, doi: 10.1016/J.ROBOT.2022.104130.
- [6] K. Parashar *et al.*, "Imaging technologies for presurgical margin assessment of basal cell carcinoma," *J. Am. Acad. Dermatol.*, vol. 88, no. 1, pp. 144–151, Jan. 2023, doi: 10.1016/J.JAAD.2021.11.010.
- [7] A. Sambri *et al.*, "Margin assessment in soft tissue sarcomas: review of the literature," *Cancers (Basel)*, vol. 13, no. 7, Apr. 2021, Art. no. 1687, doi: 10.3390/CANCERS13071687.
- [8] T. A. Moo *et al.*, "Impact of margin assessment method on positive margin rate and total volume excised," *Ann. Surg. Oncol.*, vol. 21, no. 1, pp. 86–92, Jan. 2014, doi: 10.1245/S10434-013-3257-2/TABLES/3.
- [9] S. G. Brouwer de Koning, A. W. M. A. Schaeffers, W. Schats, M. W. M. van den Brekel, T. J. M. Ruers, and M. B. Karakullukcu, "Assessment of the deep resection margin during oral cancer surgery: A systematic review," *Eur. J. Surg. Oncol.*, vol. 47, no. 9, pp. 2220–2232, 2021, doi: 10.1016/j.ejso.2021.04.016.
- [10] J. olde Heuvel *et al.*, "State-of-the-art intraoperative imaging technologies for prostate margin assessment: a systematic review," *Eur. Urol. Focus*, vol. 7, no. 4, pp. 733–741, Jul. 2021, doi: 10.1016/j.euf.2020.02.004.
- [11] R. J. Halter and Y. J. Kim, "Toward microendoscopic electrical impedance tomography for intraoperative surgical margin assessment," *IEEE Trans. Biomed. Eng.*, vol. 61, no. 11, pp. 2779–2786, Jun. 2014, doi: 10.1109/TBME.2014.2329461.
- [12] A. Mahara, S. Khan, E. K. Murphy, A. R. Schned, E. S. Hyams, and R. J. Halter, "33D microendoscopic electrical impedance tomography for margin assessment during robot-assisted laparoscopic prostatectomy," *IEEE Trans. Med. Imaging*, vol. 34, no. 7, pp. 1590–1601, Feb. 2015, doi: 10.1109/TMI.2015.2407833.
- [13] E. K. Murphy *et al.*, "Comparative study of separation between ex vivo prostatic malignant and benign tissue using electrical impedance spectroscopy and electrical impedance tomography," *Physiol. Meas.*, vol. 38, no. 6, May 2017, Art. no. 1242, doi: 10.1088/1361-6579/AA660E.
- [14] Z. Cheng, D. Dall'alba, P. Fiorini, and T. R. Savarimuthu, "Robot-assisted electrical impedance scanning system for 2D electrical impedance tomography tissue inspection," *Proc. Annu. Int. Conf. IEEE Eng. Med. Biol. Soc. EMBS*, Feb. 2021, pp. 3729–3733, doi: 10.1109/EMBC46164.2021.9629590.
- [15] A. Doussan, E. Murphy, and R. Halter, "Towards intraoperative surgical margin assessment: Validation of an electrical impedance-based probe with ex vivo bovine tissue," *Proc. SPIE 9414, Med. Imag. 2015 Comput. Diagnosis*, 2015, Art. no. 94141C. doi: <https://doi.org/10.1117/12.2082920>.
- [16] K. A. Ibrahim, M. R. Baidillah, R. Wicaksono, and M. Takei, "Skin layer classification by feedforward neural network in bioelectrical impedance spectroscopy," *J. Electr. Bioimp.*, vol. 14, pp. 19–31, 2023, doi: 10.2478/joeb-2023-0004.
- [17] M. Morin *et al.*, "Skin hydration dynamics investigated by electrical impedance techniques in vivo and in vitro," *Sci. Rep.*, vol. 10, no. 1, Oct. 2020, Art. no. 17128, doi: 10.1038/s41598-020-73684-y.
- [18] S. Ollmar and S. Grant, "Nevisense: improving the accuracy of diagnosing melanoma," *Melanoma Manag.*, vol. 3, no. 2, pp. 93–96, 2016, doi: 10.2217/mmt-2015-0004.
- [19] I. N. Rifai, M. R. Baidillah, R. Wicaksono, S. Akita, and M. Takei, "Sodium concentration imaging in dermis layer by square-wave open electrical impedance tomography (SW-oEIT) with spatial voltage thresholding (SVT)," *Biomed. Phys. Eng. Express*, vol. 9, May 2023, Art. no. 045013, doi: 10.1088/2057-1976/acd4c6.
- [20] B. Tsai, H. Xue, E. Birgersson, S. Ollmar, and U. Birgersson, "Dielectrical properties of living epidermis and dermis in the frequency range from 1 kHz to 1 MHz," *J. Electr. Bioimpedance*, vol. 10, no. 1, pp. 14–23, Jan. 2019, doi: 10.2478/joeb-2019-0003.
- [21] D. Andreuccetti, R. Fossi, and C. Petrucci, "An Internet resource for the calculation of the dielectric properties of body tissues in the frequency range 10 Hz - 100 GHz," Florence (Italy), 1997. [Online]. Available: <http://niremf.ifac.cnr.it/tissprop/>
- [22] D. Haemmerich, D. J. Schutt, A. W. Wright, J. G. Webster, and D. M. Mahvi, "Electrical conductivity measurement of excised human metastatic liver tumours before and after thermal ablation," *Physiol. Meas.*, vol. 30, no. 5, Apr. 2009, Art. no. 459, doi: 10.1088/0967-3334/30/5/003.
- [23] H. Wang *et al.*, "Dielectric properties of human liver from 10 Hz to 100 MHz: normal liver, hepatocellular carcinoma, hepatic fibrosis and liver hemangioma," *Biomed. Mater. Eng.*, vol. 24, no. 6, pp. 2725–2732, Jan. 2014, doi: 10.3233/BME-141090.
- [24] M. Rauseo *et al.*, "Electrical impedance tomography during abdominal laparoscopic surgery: a physiological pilot study," *J. Clin. Med.*, vol. 12, no. 23, Dec. 2023, Art. no. 7467, doi: 10.3390/JCM12237467.
- [25] A. Zifan, P. Liatsis, and H. Almarzouqi, "Realistic forward and inverse model mesh generation for rapid three-dimensional thoracic electrical impedance imaging," *Comput. Biol. Med.*, vol. 107, pp. 97–108, Apr. 2019, doi: 10.1016/j.combiomed.2019.02.007.
- [26] A. Adler and W. R. B. Lionheart, "Uses and abuses of EIDORS:

- an extensible software base for EIT,” *Physiol. Meas.*, vol. 27, no. 5, pp. S25–S42, May 2006, doi: 10.1088/0967-3334/27/5/S03.
- [27] M. R. Baidillah, S. Member, A.-A. S. Iman, Y. Sun, and M. Takei, “Electrical impedance spectro-tomography based on dielectric relaxation model,” *IEEE Sens. J.*, vol. 17, no. 24, pp. 8251–8262, 2017, doi: 10.1109/JSEN.2017.2710146.
- [28] U. Anushree, S. Shetty, R. Kumar, and S. Bharati, “Adjunctive diagnostic methods for skin cancer detection: a review of electrical impedance-based techniques,” *Bioelectromagnetics*, vol. 43, no. 3, pp. 193–210, Feb. 2022, doi: 10.1002/bem.22396.
- [29] H. J. Jeong, K. Kim, H. W. Kim, and Y. Park, “Classification between normal and cancerous human urothelial cells by using micro-dimensional electrochemical impedance spectroscopy combined with machine learning,” *Sensors*, vol. 22, no. 20, Oct. 2022, Art. no. 7969, doi: 10.3390/S22207969.
- [30] P. A. Sejati, B. Sun, P. N. Darma, T. Shirai, K. Narita, and M. Takei, “Multinode electrical impedance tomography (mnEIT) throughout whole-body electrical muscle stimulation (wbEMS),” *IEEE Trans. Instrum. Meas.*, vol. 72, Jun. 2023, Art. no. 4505014, doi: 10.1109/TIM.2023.3282295.
- [31] S. Huclova, D. Erni, and J. Fröhlich, “Modelling and validation of dielectric properties of human skin in the MHz region focusing on skin layer morphology and material composition,” *J. Phys. D: Appl. Phys.*, vol. 45, no. 2, Jan. 2012, Art. no. 025301, doi: 10.1088/0022-3727/45/2/025301.
- [32] S. Wang, J. Zhang, O. Gharbi, V. Vivier, and M. E. Orazem, “Electrochemical impedance spectroscopy,” *Nat. Rev. Methods Prim.*, vol. 1, no. 41, 2021, Art. no. 42, doi: 10.1038/s43586-021-00039-w.